OMB Number 3145-0058

NATIONAL SCIENCE FOUNDATION
1800 G STREET, NW
WASHINGTON, DC 20550

Exhibit A

BULK RATE
POSTAGE & FEES PAID
National Science Foundation
Permit No. G-69

PI/PD Name and Address

Charles S. Naiman
Orthogen Inc
One Irving Place
New York NY 10003

NATIONAL SCIENCE FOUNDATION
FINAL PROJECT REPORT

PART I - PROJECT IDENTIFICATION INFORMATION

1. Program Official/Org. Ritchie B. Coryell - III

2. Program Name DIV OF INDUSTRIAL INNOVATION INTERFACE

3. Award Dates (MM/YY) From: 01/92 To: 09/92

4. Institution and Address
Orthogen Inc
1 Irving Place Suite 31GI
New York NY 10003-9704

5. Award Number 9160684

6. Project Title
Joint Implant Surfaces

This Packet Contains
NSF Form 98A
And 1 Return Envelope

NSF Grant Conditions (Article 17, GC-1, and Article 9, FDP-II) require submission of a Final Project Report (NSF Form 98A) to the NSF program officer no later than 90 days after the expiration of the award. Final Project Reports for expired awards must be received before new awards can be made (NSF Grant Policy Manual Section 677).

Below, or on a separate page attached to this form, provide a summary of the completed project and technical information. Be sure to include your name and award number on each separate page. See below for more instructions.

PART II - SUMMARY OF COMPLETED PROJECT (for public use)

The summary (about 200 words) must be self-contained and intelligible to a scientifically literate reader. Without restating the project title, it should begin with a topic sentence stating the project's major thesis. The summary should include, if pertinent to the project being described, the following items:

- **The primary objectives and scope of the project**
- **The techniques or approaches used only to the degree necessary for comprehension**
- **The findings and implications stated as concisely and informatively as possible**

See attached -

PART III - TECHNICAL INFORMATION (for program management use)

List references to publications resulting from this award and briefly describe primary data, samples, physical collections, inventions, software, etc. created or gathered in the course of the research and, if appropriate, how they are being made available to the research community. Provide the NSF Invention Disclosure number for any invention.

See attached -

Charles L. Nam	11/6/92
Principal Investigator/Project Director Signature	**Date**

IMPORTANT:
MAILING INSTRUCTIONS
Return this *entire* packet plus all attachments in the envelope attached to the back of this form. Please copy the information from Part I, Block I to the *Attention block* on the envelope.

Part II—Summary of Completed Project

This study's rationale is that oriented micromachined surfaces alter the behavior of cells attached to them and that cells derived from different tissues respond differently to these surfaces. This Phase I project documents the specific in vitro effects of surface microgeometry on colony formation kinetics of rat tendon fibroblast (RTF) cells and rat bone marrow (RBM) cells. The objective is to create three types of implant surfaces: a surface that enhances bone growth and discourages soft tissue growth, to achieve good bony fixation; a surface that encourages soft tissue growth and mitigates against bone growth, to achieve soft tissue integration; and a surface that acts as a barrier to (particularly soft fibrous) tissue growth, to prevent soft tissue migration into bone attachment areas.

Different surface microgeometries, produced by microlithography, were found to cause directional RTF and RBM cell growth and control overall growth to different degrees, confirming our hypothesis that such surfaces favor one or the other type of cell growth and strongly direct that growth.

An improved, longer-lived hip arthroplasty device (as one example of a commercial application) would incorporate these differential surfaces to achieve optimal results by selectively encouraging or discouraging site-specific ingrowth of tissue types.

Note: Information marked "[PROPRIETARY]" on pp. 2, 8, 9, 10, and 21 is proprietary to Orthogen, Inc., and is to be kept strictly confidential.

RESEARCH OBJECTIVES

The overall objective of this study was to quantify the behavior of rat tendon fibroblast (RTF) and rat bone marrow (RBM) cells on oriented micromachined surfaces. The specific goals were to develop three types of surfaces with different effects on RBM and RTF cell function. The study indeed demonstrated that cells derived from these different tissue types respond differently to alternative surfaces in predictable ways. Based on these results, three types of site-appropriate surface configurations were identified that are suitable for in vivo testing.

The rationale of this study is that oriented micromachined surfaces alter the behavior of cells attached to them and that cells derived from different tissues respond differently to these surfaces. One of the coinvestigators (J. Ricci) has previously demonstrated that oriented surface microgeometry specifically influences the direction and rate of growth of cell colonies [1,2]. We also expected that cells derived from different tissues would respond differently to these surfaces. However, while these effects had been established, they have not been quantitated for different groove sizes and types of cells and tissues; nor had they been optimally applied to implant surfaces. This Phase I project sought to document the specific in vitro effects of surface microgeometry on colony formation kinetics of rat tendon fibroblast (RTF) cells and rat bone marrow (RBM) cells. This information will permit tailoring implant surfaces, on a regional level, to their tissue attachment needs.

Background. Tissue response to any synthetic implant (whether vascular device, dental implant, orthopaedic device, or any device that is in contact with soft connective or mineralized tissue) has been found to correlate with the composition, surface chemistry, and surface microgeometry of the implant material. Pilot studies of tissue response to non–resorbable, biocompatible synthetic-fiber implant materials conducted at the Hospital for Joint Diseases (HJD), demonstrated that, while the effects of small changes in composition and surface chemistry are minimal, changes in surface microgeometry exert a strong influence on cell behavior [1-5]. An extensive literature on compositional and surface chemistry effects has established certain clear relationships—e.g., materials with high surface free energies (as defined by contact angle studies) exhibit better cell attachment and growth characteristics in vitro [6,7]. At the same time, many of these same studies (as well as publications from HJD have demonstrated that many materials with very different initial surface free energies exhibit similar cell responses in the presence of serum proteins [3-6,8,9], implying that initial surface free energies are not a dominant factor in tissue response to implants in vivo.

This is not to dismiss the fact that surface chemistry and surface energy may determine the type, distribution, configuration, and turnover of proteins at the implant surface [10]. The implant surface is clearly an area of complex and dynamic physical chemistry, and immune response to implants is influenced by (and contributes to) the complexity of this system [11]. The point—in keeping with the central design tool of this proposal—is rather that implant surface microgeometry is an influence that "superimposes" itself on these other factors.

The microtextured surfaces initially studied are comprised of well-characterized unidirectionally oriented (striated) structures of selected sizes and geometries. Custom substrates were molded from templates precision-fabricated at the National Nanofabrication Facility at Cornell University and sputter-coated with a 600-Å layer of TiO_2 to simulate the orthopaedic implant material surface. Ti coupons were also successfully fabricated by laser; their use for cell growth, beyond the scope of these Phase I experiments, will be advantageous for in vivo testing. Laser-micromachining will eventually be used to apply the microgeometries developed in this study onto implant surfaces. Time and cost constraints made it infeasible to use the laser technique for our pilot study. In addition, it was technically necessary to visualize the cell colonies on these surfaces in order to measure their growth; this can be accomplished on polymer substrates coated with titanium oxide, but is extremely difficult on solid metal surfaces.

Cell colony growth was evaluated using rat tendon fibroblast (RTF) cells and rat bone marrow (RBM) cells. A straightforward, easily replicable colony outgrowth model developed in the Department of Bioengineering of the Hospital for Joint Diseases (HJD) [1-3] permits detailed evaluation of colony growth rates (through colony size) and direction of colony growth (through measurement of colony shape). Comparison of growth of colonies of each cell type, rather than the use of mixed colonies, was conducted because of the difficulties involved with RBM vs. RTF cell identification in large, mixed-population cell colonies. Using appropriate models, dose-response relationships have been established between surface geometric size/shape parameters and cell colony formation parameters.

Objectives. The purpose of this study was to selectively create three types of hip stem implant surfaces: (1) a surface that enhances bone growth and discourages soft tissue growth, to achieve good bone fixation in the proximal region; (2) a surface that encourages soft tissue growth and mitigates against bone growth, to achieve soft tissue integration in the distal region; and (3) a surface that acts as a barrier to tissue growth, particularly soft fibrous tissue growth, to prevent soft tissue migration from the distal region into the bone attachment area; this will consist of a microtexture that causes strong fibrous tissue interdigitation.

[PROPRIETARY]

A resulting hip arthroplasty device takes into account the following considerations: (1) press-fit implants afford good contact in the medial and lateral regions, but not in the anterior and posterior regions; (2) it is desirable to achieve bony fixation in the proximal region and to discourage it in the distal region; (3) it is desirable to exclude fibrous tissue from entering the bone attachment regions. Consistent with these is a design incorporating a microgrooved finish on the distal stem that is optimized for soft tissue formation, another microconfiguration on the proximal stem for optimal bone attachment, and a third microgrooved "barrier zone" on the neck to prevent fibrous tissue ingrowth, as shown in Figure 1. (Figures are grouped at the end of this report.)

The information obtained in Phase I will be used to design, construct, and test a micromachined implant surface during Phase II using an implantable chamber model designed in the HJD Bioengineering laboratory for in vivo testing [12,13]. During Phase II, these surfaces will also be tested using a modular canine press-fit hip design that allows interchangeable surfaces on different parts of the femoral component [14]. The surface will

then be applied to a human press-fit hip joint prosthesis to optimize bone attachment where desired. Computer-controlled laser machining techniques can be used to rapidly and cost-effectively produce the surface geometries developed in Phase I.

DESCRIPTION OF RESEARCH

Several materials and experimental techniques have been used throughout the experiments, as outlined in the following sections. The rationale for use of these methods is based on literature accounts and past experience concerning these techniques and models.

Substrate Fabrication. These studies were performed using a square wave shape and a flat surface as a control (produced by the same methods), since the square wave shape has demonstrated a strong effect of cellular contact guidance in past studies [15].

Following the nomenclature of Cheroudi et al. [16] for the surfaces, the distance comprising one groove and one ridge between the grooves is called the *repeat spacing*, or *pitch* ($a + b$, in Table 1). The *depth* (c in Table 1) of the groove refers to its deepest point, and the *width* (b in Table 1) is the total opening in the plane of the substrate.

It has previously been observed that the cell cytoskeleton controls cell attachment and shape as well as cell response to surface microgeometry (contact guidance). It is expected that normal cell size and shape will determine which surface microgeometry sizes will have the greatest influence on cell attachment, orientation, and growth. It was therefore expected that the greatest differentiation in cell response to surface microgeometry would be seen in the 3- to 10-μm region that approximately brackets the width of the cell body in different attachment states. It was thus presumed that the most important "design rules" for a given cell type would occur in this region.

The substrates used in these experiments have been molded from templates precision-fabricated at the National Nanofabrication Facility (NNF) at Cornell University. The investigators fabricated the templates with the assistance of the staff at NNF.

Fabrication of the microstructures by microlithography is a three-step process: design, application of a thin photoreactive layer, and development. To model a square-wave architecture, a window with parallel grid lines was designed on the CAD program Symbad. CAD files were used to store different grid dimensions. Via a VAXstation-3100, these files were transferred to an Optical Pattern Generator (GCA PG3600F) to fabricate a photomask from the design layout. This was done by exposing the window on a high-resolution emulsion plate with a laser interferometer. All photomasks were developed by typical film development procedures.

In the next process, 3-in. silicon wafers were coated with 15 μm of silicon dioxide, obtained by a mixture of 70% nitrous oxide and 17% silane gas, on a Chemical Deposition System (IPE Model 1000). Deposition took place at a rate of 40 nm/min, with chamber conditions of 450 mtorr pressure, 50 W reflecting power, and 200°C temperature. To align each grid window, the wafers were placed on a Projection Mask Aligner (GCA 4800 DSW) with their respective masks. For each template, there was a total of 239 exposures for 1.2 sec each. Exposure subsequently applied a thin layer of photoresist.

The development of square-wave microstructure was achieved by multiple reactive ion etching (RIE) techniques. Each template was initially placed on the Magnetron Ion Etcher (MCR Model 720) where the silicon dioxide surface was etched with carbon tetraflouride

at 1.0-kW peak voltage. Templates were next placed on the Barrel Etcher (IPC P2000) to strip the photoresist at 13.5 torr pressure and 240°C temperature. The bare polysilicon surface was further etched with the Plasma Therm RIE System (PK 1250). This system etches in a directional manner, producing the square-wave shape used in these studies. The parameters used were 49 parts/cm^3 (pccm) chlorine and 7 pccm boron trichloride, 60 mtorr pressure, and 200 kW reflecting power. Finished templates were washed in hydrochloric acid and attached to 3-in.-diameter aluminum stubs using epoxy to provide a rigid base. One-half of each template received an experimental microtexture, the other half left flat. An example of a microtextured surface is shown in Fig. 2.

Culture plate surfaces were created from the templates by solvent casting. The mold solution was obtained by dissolving 15 g of polystyrene in 100 mL ethyl acetate for at least 6 hr. A dam was produced by attaching tape around the perimeter of the template. An 8-mm solvent depth produce 0.5-mm polystyrene substrates. After pouring the solvent on the template and before allowing it to dry, they were placed under high vacuum for 1 min to eliminate air bubbles at the interface. Air bubbles were shown to produce inconsistencies in the experimental surfaces. The solvent was allowed to dry for 24 hr and the surfaces were placed in a water bath for 5 hr. The substrates were peeled off their respective templates, and outer edges were removed to yield 50-mm circles. Substrates were allowed to dry for at least 24 hr to completely remove the solvent.

Surfaces were then evaporation-coated with titanium oxide in a Denton 502 Vacuum Evaporator. To obtain a 600-Å coating, substrates were placed 100 mm from the electrodes under a 40-kW reflecting power and 5×10^{-5} mtorr pressure. Substrates were ethanol-sterilized for 5 min and attached to 50-mm petri dishes with a heated probe.

Preparation of Rat Tendon Fibroblast (RTF) Cell Cultures from Explants. To initiate RTF cell cultures, hindfoot extensor tendons were removed from male, 14-day-old Sprague-Dawley rats that had been sacrificed by CO_2 overdose. This is a painless method of sacrifice and does not contaminate the tendon tissue. Four extensor tendons were removed under sterile conditions from each foot and placed in Hank's balanced salt solution (HBSS) containing 1% penicillin-streptomycin. The tendons were then separated from sheath tissue by microdissection. All culture procedures were conducted under sterile conditions. Cultures were grown in a 37°C incubator in an atmosphere consisting of 95% air, 5% CO_2, and saturated humidity. Cultures were maintained with Dulbecco's Modified Eagle's Medium (DMEM) containing 10% fetal bovine serum and 1% pen-strep. The medium was carefully maintained at pH 7.4 .

Subculturing Procedure for RTF Cell Cultures. Groups of explant cultures were grown for approximately 12-17 days; explants were removed, and the cultures were subcultured by enzyme digestion. Cultures were treated with a 0.25% trypsin solution in calcium- and magnesium-free HBSS for 20 min in order to free the cells from the culture plates. Cells were rinsed in medium containing 10% serum to stop the trypsin reaction, counted using a hemocytometer, and used to inoculate culture plates or initiate dot cultures. To ensure that the cells retained their in vivo behavior characteristics, only primary, secondary, and tertiary cultures were used for the experiments.

Preparation of Rat Bone Marrow (RBM) Cultures from Rat Femurs. Cell cultures were prepared from 14-day-old rat femurs according to the method of Maniatopoulos [17] In brief, femurs were dissected out under sterile conditions and the ends cut off. The mar-

row cavity was flushed out with medium using a syringe and the contents were incubated in a culture plate. While the hemopoietic elements do not attach, the stromal cells attach to the plate. After the unattached elements were removed, the attached cells were allowed to grow to confluency. The cells routinely stained positive for alkaline phosphatase activity. All experiments were conducted in DMEM with 10% fetal calf serum and 1% penstrep. A similar model has previously been used successfully to study in vitro mineralized tissue formation on titanium surfaces [18]

Subculturing Procedure for RBM Cultures. When these cultures became confluent, they were subcultured using the same procedure described for the RTF cultures.

Initiation of Radiating "Dot" Cultures. RTF and RBM cells were embedded in a collagenous matrix as a source of cell colonies. These cultures were initiated by mixing cell suspensions with pepsin-digested type I bovine collagen solution (Vitrogen 100, Collagen Corporation). This solution is dispensed as 2-μL aliquots (containing 18,000-20,000 cells each) on the control and experimental substrates and polymerized to form gels. Eight colonies were formed on each experimental substrate (designed to fit in a 60-mm culture plate) with four colonies placed on the flat control side and four colonies placed on the experimental microgeometry side. The resulting gel "dots" acted as sources of cells for colony formation. The cultures were maintained under standard sterile conditions in the appropriate medium.

Cultures were examined using a Wild inverted-phase contrast microscope with Olympus 35mm camera attachment.

The "dot" culture model is basically an explant model with some important distinctions. While explant cultures can be used to measure cell colony formation of surfaces [19], they tend to form irregular colonies whose shapes cannot be easily analyzed. This is because the explants tend to be variable in shape, cell number, and area of contact with the substrate. In the present model, colony formation begins from a circular dot of cell-containing collagen gel. Colony cell numbers and shapes are consistent; colony formation kinetics are consistent and easily measured. Furthermore, work at HJD has demonstrated that whereas colony formation on flat substrates results in circular colonies, on striated surfaces differential growth predominantly parallel to the striations results in elongated colonies [1,2]. It is the consistency and measurability of this model that makes it appropriate for these experiments.

The investigators believe that it is important to use freshly isolated cells for experiments such as these, since continuous cell lines, transformed cell lines, and cells that have been subcultured through many passages do not exhibit attachment and migration behavior that is true to their normal in vivo state.

Measurement of Radiating Cultures. Cultures were preserved in 10% phosphate-buffered formalin on days 4 and 8 and stained with toluidine blue stain. Representative cultures were viewed and photographed using light microscopy in order to examine individual cells as well as colony outgrowth patterns. Using the Scientific Imaging Solutions computer workstation (Biological Detector Systems, Inc., Bethesda, MD), which consists of a light microscope (Leitz Orthoplan or Wild MC3 stereomicroscope) with an MTI CCD72 videocamera connected to a Macintosh IIfx personal computer with Perceptics video acquisition hardware and TCL-Image image processing/image analysis software, images of the colonies were digitized and measured. Overall colony area and aspect ratios

relative to the material surface microgeometry were recorded.

RESULTS

Characterization of Experimental Substrates: Analysis of Surface Microgeometry. The dimensions of the square-wave surface microgeometries were measured using the Scientific Imaging Solutions Workstation. Groove spacing was determined with the light microscope system, and this measurement was used to calibrate a JEOL JSM T300 scanning electron microscope (SEM). Depth of waves was determined by comparison of photomicrographs of the surfaces at 0° and tilted at a 45° angle. Observations from these instruments revealed slightly different microstructure dimensions than expected (see Table 1). Several steps in the microlithography process are believed to have contributed to this overall error. For example, the distance of the masks from the lens in the Projection Mask Aligner might not conform accurately to those set at its computer interface. Despite the departure from original dimensions, approximate square-wave microstructure was still obtained, since the etch depth, which is a function of the constant etch rate and time, was controlled. Note that the 15-μm depth could not be achieved by the suggested procedure because etching beyond 8 μm produced an uneven surface. Therefore, those templates with greater than 8-μm grids exhibit rectangular-wave shapes instead of square-wave shapes. Ti coupons were also processed by laser, achieving a wide variety of similar shapes. Considerable experience was gained on laser system parameter control for shaping microtextures. (Dot culture studies with these materials were beyond the scope of Phase I.)

Table 1: Expected and actual dimensions of the square-wave microstructures

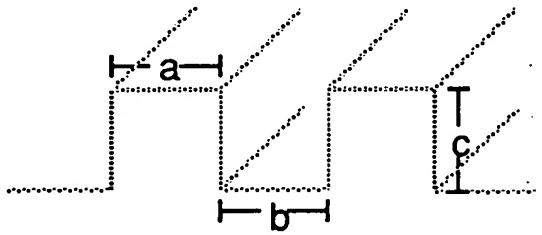

Template	Expected Dimensions (μm) (a x b x c)	Actual dimensions (μm) (a x b x c)
1	2.0 x 2.0 x 2.0	1.80 x 1.75 x 1.75
2	4.0 x 4.0 x 4.0	3.50 x 3.50 x 3.50
3	6.0 x 6.0 x 6.0	6.50 x 6.33 x 5.00
4	8.0 x 8.0 x 8.0	8.00 x 7.75 x 7.50
5	10.0 x 10.0 x 10.0	10.00 x 8.00 x 7.75
6	15.0 x 15.0 x 15.0	12.00 x 11.50 x 7.50

Note: In order to simplify nomenclature, the substrates used in these studies will be referred to as 2 μm (a = 1.80 μm), 4 μm (a = 3.50 μm), 6 μm (a = 6.50 μm), 8 μm (a = 8.00 μm), and 12 μm (a = 12.00 μm).

Cell Colony Initiation. In this series of studies RTF and RBM cell colonies were grown on each of the six experimental and control substrates listed earlier. RTF and RBM cells from the same animals were used to initiate groups of five to eight substrates per microgeometry type and cell type. Each surface had a flat area to act as an internal control. Four colonies each were initiated on the flat control and experimental sides of each 55-mm-diameter substrate. Thus 40-64 colonies were initiated on each type of substrate for each cell type, divided between flat control surfaces and experimental microgeometry surfaces. Earlier experiments indicated that there is a 1- to 3-day lag period, depending on cell type, before consistent colony growth is established [1,2]. These experiments indicated that the colonies grew consistently after this period and that cell colony diameters increased in a linear fashion between days 3 and 12. Thus, the colonies analyzed in these experiments were fixed and quantitated at 4 and 8 days in order to document the most consistent period in colony growth. The RTF and RBM cell colonies were measured for area, *x*-axis growth (parallel to surface microgeometry), and *y*-axis growth (perpendicular to surface microgeometry). In order to correct for small variations in initial colony size and shape, which can be affected by the way the shape of the liquid collagen drop is influenced by surface microgeometry, average colony parameters at 4 days are subtracted from the 8-day data for each cell type and surface. This yields data expressed as area, *x*-axis, or *y*-axis increase between 4 and 8 days. *X*- to *y*-axis growth ratios and RBM cell vs. RTF cell growth ratios are also used to compare these results.

Cell Growth on Control Surfaces. Both cell types showed consistent growth by day 4, with the RTF cells showing earlier growth than the RBM cells. A 4-day-old RBM cell colony is shown in Fig. 3. The central region shows the original "dot," consisting of collagen and cells. Cell outgrowth is seen at the periphery, with the cells oriented randomly and becoming sparse at the periphery. Both cell types showed extensive growth between 4 and 8 days, with the RTF cells growing at a faster rate than the RBM cells (Figs. 4, 5).

Cell Orientation and Migration. The experimental surfaces caused oriented cell attachment and migration, resulting in elongated colony growth (Figs. 6 and 7), which was accelerated in the *x*-direction (parallel to the surface microgeometry) and inhibited in the *y*-direction (perpendicular to the surface microgeometry; Figs. 8-11). On an individual cell level, the cells were observed to orient along the surface grooves (Fig. 7). This causes the cells to be "channeled" in the *x*-direction, as compared with control cultures, where the outgrowing cells move randomly on the flat surfaces. The most efficient cell "channeling" was observed on the 6-μm and 8-μm surfaces. On these surfaces, both cell types were observed to attach and orient within the grooves and on flat tops of the grooves (Fig. 7). This resulted in enhanced *x*-axis growth and almost no *y*-axis growth by both cell types on these surfaces. On the smaller microgeometries, a different effect was observed. Both the RBM and RTF cells bridged the surfaces of the 2-μm grooves (Fig. 12) resulting in cells with different morphologies than those on the 6-, 8-, and 12-μm surfaces. These cells were wide and flattened and were not well oriented. On the 4-μm grooves, the RBM and RTF cells showed mixed morphologies, with most cells aligned and elongated but not fully attached within the grooves. This resulted in appreciable *y*-axis growth by the RBM cells on the 2-μm surfaces and by the RTF cells on the 2- and 4-μm surfaces. At the other end of the size range, limited *y*-axis growth was also observed when these cell types were grown on the 12-μm surfaces. This may be a result of the mi-

crogeometry being significantly larger than the cell dimensions, allowing some diagonal cell orientation and cell "wraparound," resulting in limited *y*-axis growth (Fig. 13).

Microgeometry Effects on Overall Cell Colony Growth. The results of the observed effects of these surfaces on overall RBM and RTF cell colony growth was very pronounced. All the experimental substrates caused varying but significant increases in *x*-axis growth compared to the diameter increase of the controls and varying but pronounced inhibition of *y*-axis growth (Figs. 8-11). This nearly always resulted in suppression of overall growth of the RBM and RTF cell colonies compared with controls (Figs. 4 and 5). The exception was RTF cell growth on the 2-μm surface (Fig. 5), which was equivalent in area increase to controls, presumably because of the *y*-axis growth contribution seen in Fig. 11. Importantly, suppression of cell growth differed between cell types. This offers the opportunity to differentially provide a growth advantage to one cell type over the other.

The Basis of Microgeometric Growth Control. The observed growth suppression is a geometric phenomenon. Circular control colonies increase in area as a function of the square of their radius. The colonies grown on the microgeometry surfaces become rectangular-to-oval in shape because of differential *x*- and *y*-axis growth rates. Since *y*-axis growth is extremely low in most cases, the colonies increase significantly in area only in the *x*-direction. This results in area increase based almost solely on linear increase in *x*-axis length. This one-dimensional growth (as compared to the two-dimensional growth of circular controls) results in a slower linear rate of area increase, even though its *x*-axis growth is faster than that of the control diameter growth.

[PROPRIETARY]

SELECTION OF POTENTIAL IMPLANT SURFACES

The aim of this portion of the study was to develop three types of surface microgeometries with different effects on RBM and RTF cell function.

Barrier Zone Surface—to Direct Growth of Fibrous Tissue. This surface should prevent *y*-axis migration and growth and orient fibrous tissue. While the maximal orientational effect (highest *x*-axis/*y*-axis ratio) on the RBM cells was observed on the 6-, 8-, and 12-μm surfaces (Fig. 14), the maximal effect on the RTF cells was observed on the 8-μm surface (Fig. 15). This indicates that the best microgeometry size to act as a barrier for RTF cell growth would be the 8-μm surface, since RTF cells grown on this surface would have the smallest *y*-axis growth across this surface and an enhanced directional growth in the *x*-axis to values nearly twice those of controls (Figs. 11 and 15).

Surfaces for Stimulation of Fibrous Tissue Growth. Since fibrous tissue and bone cells will be "competing" for these surfaces in vivo, the ratio of RBM to RTF colony area increase on a given surface is an important parameter in surface selection. This ratio indicates the relative stimulation or inhibition of cell growth on these surfaces (Fig. 16). Theoretically this ratio would be significant to provide advantage for growth of one or the other cell type on a surface, with high ratios favoring bone cell growth and low ratios favoring fibrous tissue growth. Based on these ratios, the 2-μm surface would provide a 32.8% decrease in RBM/RTF growth, providing a significant advantage in RTF cell growth. This surface could be used to favor RTF cell growth; it can also be used to significantly orient growth of these cells. The 4-μm surface provides a similar ratio but is based

[PROPRIETARY]

on lower overall growth rates (Figs. 4 and 5). If nonoriented fibrous cell growth is required, the flat control surface provides an inherent advantage to RTF cells (a ratio of RBM to RTF cell growth of approximately 0.6). This effect has been observed in vivo [13] where smooth surfaces have been shown to favor formation of thick fibrous tissue capsule formation as compared to textured surfaces of the same composition, which show less fibrous capsule formation and more extensive osteointegration.

A Surface for Stimulation and Directional Conduction of Bone Growth. The surface with the highest ratio of RBM to RTF cell growth is the 12-μm substrate. The basis for the ratio is the fact that this surface inhibits RTF colony growth by 53.1% relative to controls (Fig. 5). This is close to the maximal suppression of RTF cell growth seen on these microgeometries. This same surface, however, does not maximally suppress RBM cell growth (46.3% suppression relative to controls, Fig. 4). This differential suppression results in a 14.4% increase in RBM/RTF growth ratio relative to the control ratio (Fig. 16). In vivo, where both cell types are present and compete for growth, this provides a significant advantage to RBM colony growth. RBM cells grown on this surface also exhibit greatly enhanced directional growth in the *x- axis*. In vivo, this surface should favor bone over soft tissue growth and could be used to directionally conduct bone growth.

TECHNICAL IMPLICATIONS

Based on the studies documented above, three types of site-appropriate surface configurations were identified that are suitable for in vivo testing:

Barrier Zone Surface—to Direct Conduction of Soft Tissue. The 8-μm surface, which effectively eliminates *y*-axis growth and stimulates *x*-axis growth in fibrous tissue cells, can be used as a barrier zone to prevent fibrous tissue migration and/or can be used to directionally conduct fibrous tissue.

Enhanced Fibrous Tissue Growth Surface. The 2-μm surface can be used to stimulate fibrous tissue growth relative to bone cells. It has the additional advantage of causing specific directional migration at more than twice the rate of cells on the flat controls. In areas of an implant surface where a randomly oriented fibrous tissue layer is needed, and no directional conduction is necessary, the flat surface, which inherently favors fibrous versus bone cell growth, can be used.

Enhanced Bone Growth Surface—to Direct Conduction of Bone Tissue. The 12-μm surface has been shown to increase the RBM/RTF cell growth ratio. This favors bone cell growth over fibrous tissue growth. In addition, this surface causes specific directional migration of bone cells at approximately twice the rate of cells on the flat surface. This surface can be used to enhance bone vs. soft tissue growth as well as direct bone growth into regions of an implant surface where bone fixation is needed.

TECHNICAL FEASIBILITY

The nature of laser-generated microtextures permits them to be remotely imprinted on the implant surface using the same fixturing and computer coordinates already derived for

[PROPRIETARY]

macrofabrication. Several commercially available and proposed implants have complex surface microgeometries, an important parameter that has not been adequately examined. In order to focus on this parameter, this study has (1) eliminated the influence of immune response by conducting experiments in vitro; and (2) factored out the effects of surface chemistry and surface free energy by employing one, well-characterized material in the construction of all substrates and conducting all experiments in the presence of serum proteins. This approach allowed the study to focus on the influence of surface microgeometry on cell growth and migration.

The ability of surface microgeometry to influence cell and tissue formation—both bone and soft tissue—has already been demonstrated. The requisite laser micromachining techniques are also available. What remains to be developed are design parameters for regional surface microgeometries that will selectively optimize tissue interaction with the implant surface. Proper bone and soft tissue interaction will result in optimal stress transfer to the femoral cortical bone and thus minimize bone resorption and loosening—typical complications that compromise the integrity of an implant and shorten its effective life.

A detailed profile of the effects of the selected sizes and shapes of surface microgeometry on cell function will facilitate the accomplishment of these design objectives.

In addition to the in vitro testing, we have developed prototype laser-micromachined titanium-alloy surfaces, demonstrating that the surface microgeometries developed in this study can be applied to implant surfaces. Under contract and direction by Orthogen scientists, Texas Laserworks (Waco, Texas) has used laser micromachining to produce surface microgeometry on titanium alloy (6% aluminum, 4% vanadium) templates. This alloy is routinely used to construct orthopaedic implants. Surfaces with features ranging from 3-μm grooves (Fig. 17) to 25-μm grooves (Fig. 18) were produced using various laser parameters. These prototypes demonstrate the feasibility of applying this technology to an orthopaedic implant surface.

In Phase II, laser-micromachined metal implant surfaces with surface microgeometries developed in this study will be further developed and tested in an in vivo implantable chamber model, developed at HJD, for testing tissue interaction with implant surfaces [12,13]. These surfaces will then be applied to actual hip implants for testing in a canine total hip replacement model that allows comparative testing of bone and soft tissue response different femoral stem surfaces [14].

POTENTIAL APPLICATIONS

Bone implants often loosen due to the invasion of fibrous tissue. The transformation from bone attachment to fibrous encapsulation is governed by surface chemistry, strain, and microgeometry. The ability to control tissue migration at an implant surface through surface microgeometry—specifically, to shift the equilibrium away from fibrous encapsulation and toward bone integration—is of significant clinical value.

The enhanced design of bone attachment surfaces for joint implants will provide an improved, marketable product. Over 400,000 total hip arthroplasties are performed annually worldwide. The field of orthopaedic joint implants is currently projected to grow at

20% per year over the next 10 years. As these devices are increasingly used in younger, more active individuals, improved noncemented surfaces will be needed in an ever-increasing proportion of these implanted devices.

REFERENCES

1. Ricci JL, Wang P, Zakow P, Howard C, Alexander H: Tendon and bone cell colony formation on striated surfaces: a model for in vitro examination of cell response to different surface textures and geometries. Trans Soc Biomat 17: 253, 1991.
2. Ricci JL, Alexander H, Howard C: The influence of surface microgeometry on fibroblast colonization of synthetic surfaces. In: Tissue-Inducing Biomaterials, Materials Research Society Symposium Proceedings Vol. 252, edited by L. G. Cima and E. S. Ron, Materials Research Society, Pittsburgh, Pennsylvania. pp. 221-229, 1992.
3. Ricci J, and Alexander H: In vitro tendon cell growth on synthetic fiber implant materials: biological implications. Bull Hosp Joint Dis Orthop Inst 50(2):126-138, 1990.
4. Ricci JL, Gona AG, Alexander H, Parsons JR: Morphological characteristics of tendon cells cultured on synthetic fibers. J Biomed Mater Res 18:1073-1087, 1984.
5. Ricci JL, Gona AG, Alexander H: In vitro tendon cell growth rates on a synthetic fiber scaffold material and on standard culture plates. J Biomed Mater Res 25(5): 651-666, 1991 .
6. Shakenraad JM, Busscher JH, Wildevuur CRH, Arends J: The influence of substratum surface free energy on growth and spreading of human fibroblasts in the presence and absence of serum proteins. J Biomed Mater Res 20:773-784, 1986.
7. van der Valk P, van Pelt AWJ, Busscher HJ, de Jong HP, Wildevuur CRH, Arends J: Interaction of fibroblasts and polymer surfaces: relationship between surface free energy and fibroblast spreading. J Biomed Mater Res 17:807-817, 1983 .
8. Horbett TA, Schway MB: Correlations between mouse 3T3 cell spreading and serum fibronectin adsorption on glass and hyroxyethylmethacrylate-ethylmethacrylate copolymers. J Biomed Mater Res 22:751-762.
9. van Wachem PB, Vreriks CM, Beugeling T, Feijen J, Bantjes A, Detmers JP, van Aken WG: The influence of protein adsorption on interactions of cultures human endothelial cells with polymers. J Biomed Mater Res 21:701-718, 1987.
10. Lenk TJ, Ratner BD, Gendreau RM, Chittur KK: IR spectral changes of bovine serum albumin upon surface adsorption. J Biomed Mater Res 23:535-548, 1989.
11. Miller KM, Anderson, JM: Human monocyte/macrophage activation and interleuken 1 generation by biomedical polymers. J Biomed Mater Res 22:713-731, 1988.
12. Spivak JM, Ricci JL, Blumenthal NC, Alexander H (1990) A new canine model to evaluate the biological response of intramedullary bone to implant materials and surfaces. J Biomed Mater Res 24:1121-1149.
13. Ricci JL, Spivak JM, Blumenthal NC, Alexander H: Modulation of bone ingrowth by surface chemistry and roughness. In: The Bone-Biomaterial Interface, edited by JE Davies, University of Toronto Press, Toronto, Ont. Canada. pp. 334-349, 1991.
14. Poser RD, Magee FP, Kay JF, Toal TR, Hedley AK: Biomechanical and histologic assessment of HA enhanced long-term fixation in a unique loaded canine implant. Fourth World Biomater Congr, Berlin, April 24-28, 1992.

15. Clark P, Connolly P, Curtis ASG Dow JAT, Wilkinson CDW: Topographical control of cell behavior. II. Multiple grooved substrata. Development 108:635-644, 1990.
16. Chehroudi B, Gould TRL, Brunette DM: Effects of a grooved titanium-coated implant surface on epithelial cell behaviour in vitro and in vivo. J Biomed Mater Res 24:1067-1085, 1990.
17. Maniatopoulous C, Sodek J, Melcher AH: Bone formation in vitro by stromal cells obtained from bone marrow of young adult rate. Cell Tiss Res 254:317-330, 1988.
18. Davies JE, Lowenburg, B, Shiga A: The bone-titanium interface in vitro. J Biomed Mater Res 24:1263-1288, 1990.
19. Duval JL, Letort M, Sigot-Luizard MF: Comparative assessment of cell/substratum static adhesion using an in vitro organ culture method and computerized analysis system. Biomaterials 9:155-161, 1988.

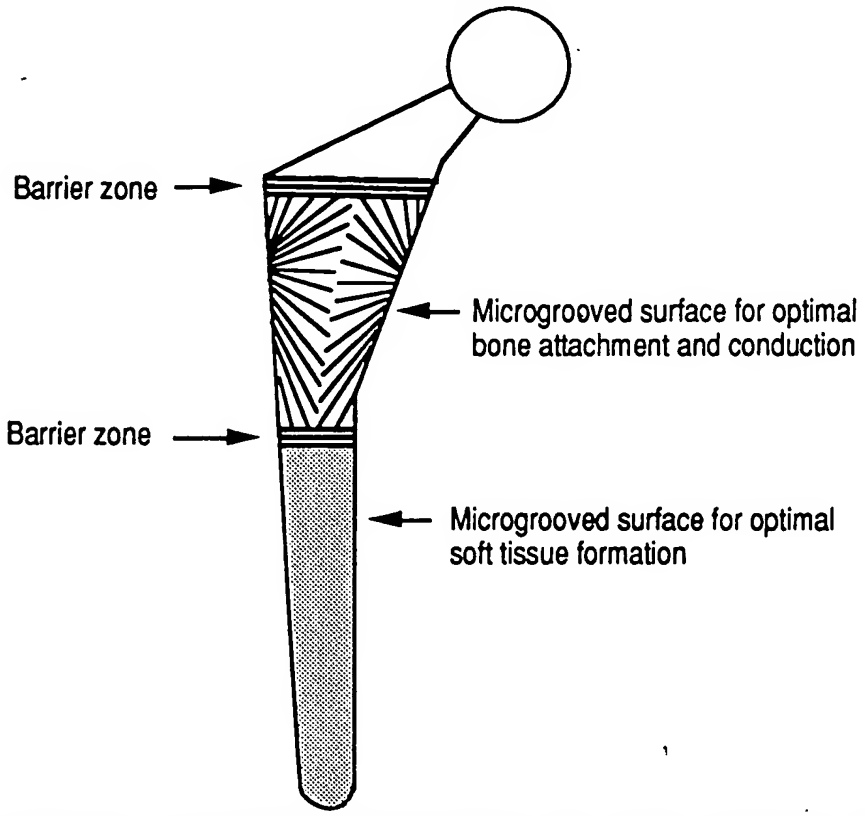

Fig. 1. Schematic diagram of a proposed femoral component with zones of different surface micro–geometries aimed at encouraging and/or conducting bone growth or soft tissue growth. The barrier zones prevent soft tissue from migrating into bone attachment areas. *Note:* Surface microgeometries are schematically represented and are not drawn to scale.

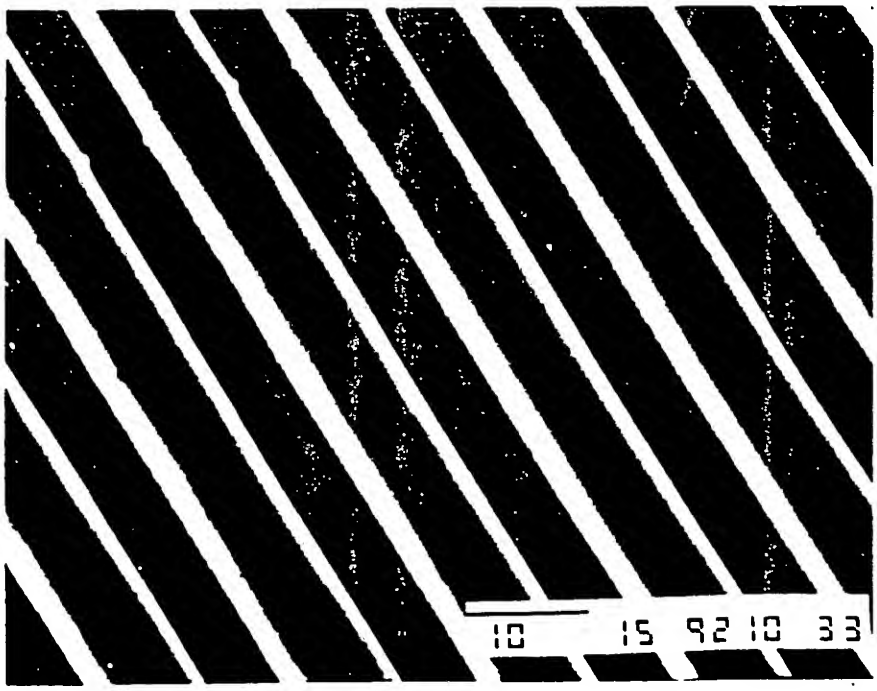

Fig. 2. Scanning electron micrograph of a mold used to produce 6-μm surfaces. The surface was photographed at an angle of approximately 30° to show its square-wave configuration. Note the smooth finish of the etched grooves. Bar = 10 μm.

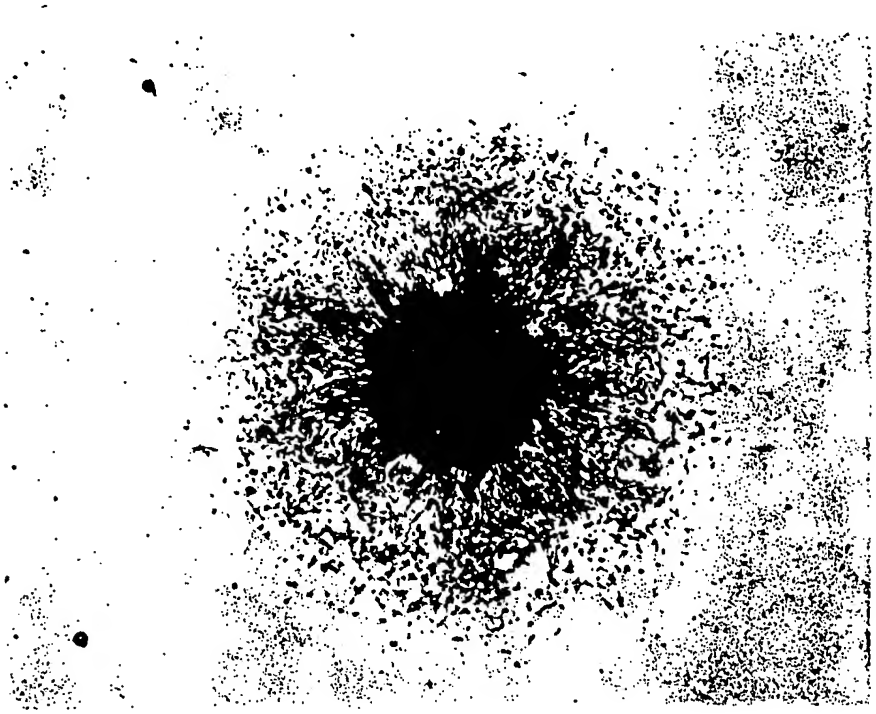

Fig. 3. Light micrograph of a circular RBM cell colony on a flat control surface after 4 days. The "dot" of collagen and cells that was used to initiate the colony is visible at the center. The colony is approximately 6 mm in diameter.

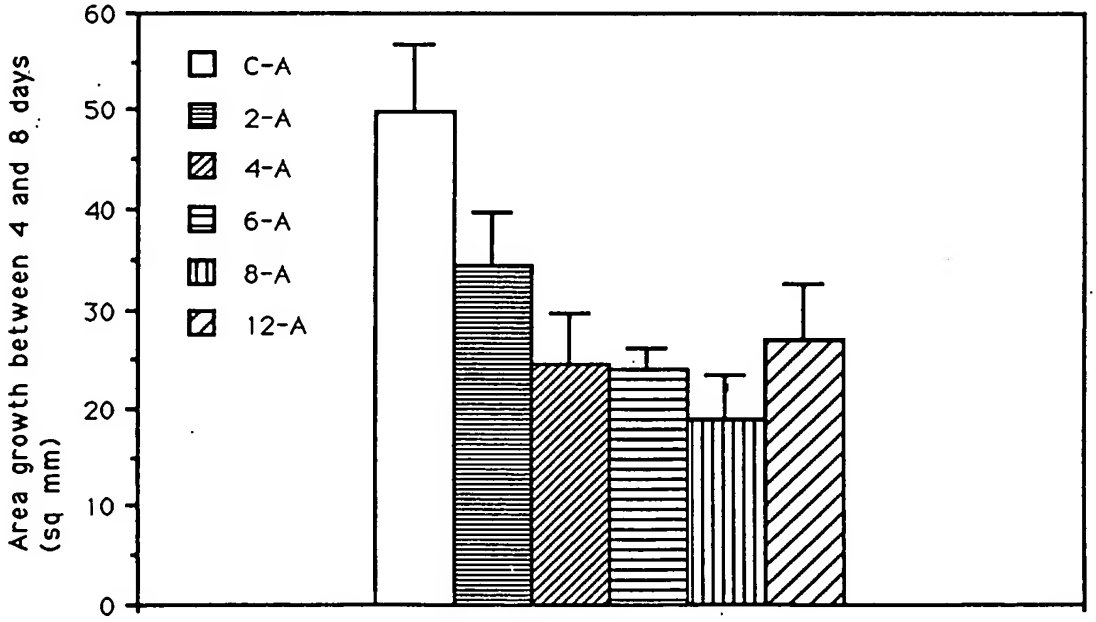

Fig. 4. Graph of RBM colony area increase between 4 and 8 days on the control (C-A) and micro-geometry surfaces (2-μm surface = 2-A). Student's *t*-test indicated that the control colonies were different from all other colonies at a statistical level of $p < .001$. The 2-μm colonies were different from the 4-, 6-, and 8-μm colonies at a level of $p < .05$, but were not significantly different from the 12-μm colonies. (Error bars = S.D.)

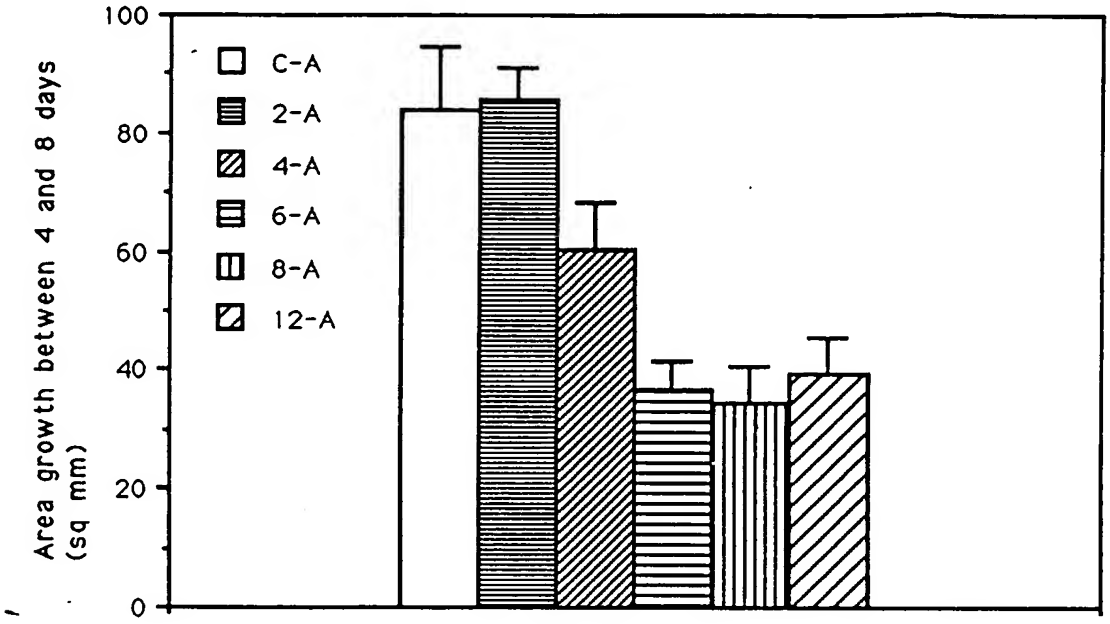

Fig. 5. Graph of RTF colony area increase between 4 and 8 days on the control (C-A) and microgeometry surfaces (2-μm surface = 2-A). Student's *t*-test indicated that the control and 2-μm colonies were different from the 4-μm surface at a level of $p < .001$. The 4-μm surface was different from the 6-, 8-, and 12-μm surfaces at a level of $p < .01$. (Error bars = S.D.)

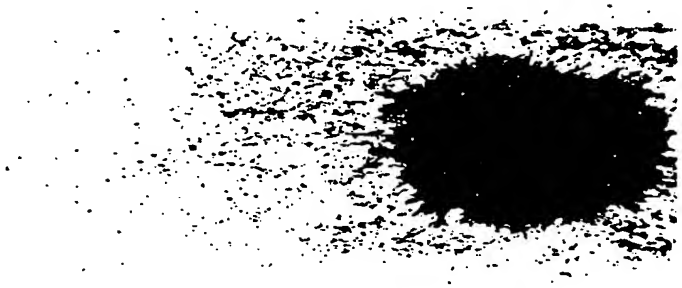

Fig. 6. Light micrograph of an RBM cell colony on a 4-μm surface after 4 days. Cell growth has occurred primarily parallel to the surface microgeometry (not visible at this magnification). This photomicrograph was taken at the same magnification as Fig. 3 for comparison.

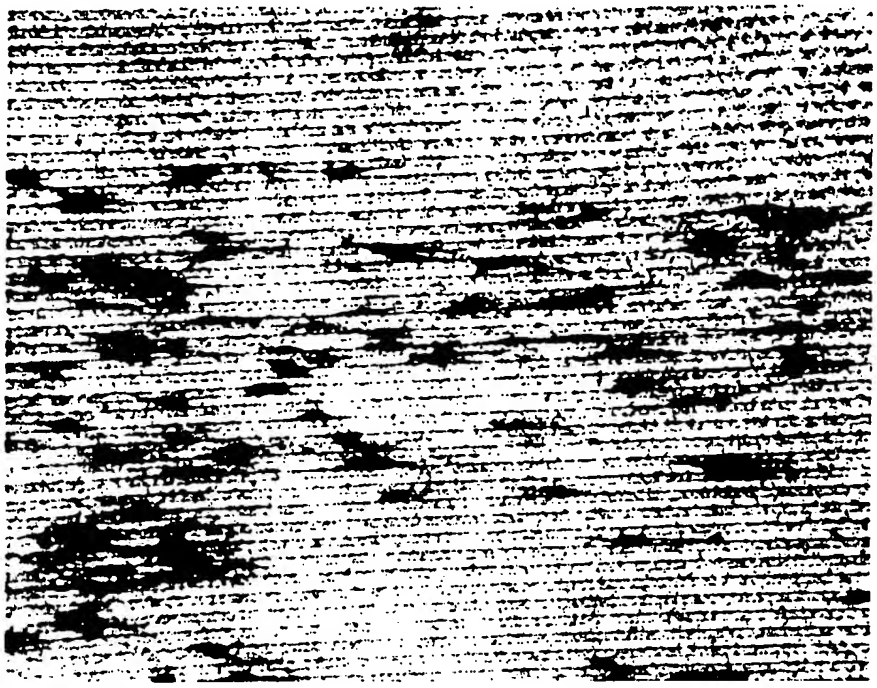

Fig. 7. Light micrograph of an RBM cell colony on a 6-μm surface after 4 days. The majority of cells are aligned parallel to the surface microgeometry. Some of the cell bodies are within grooves, while others are attached on ridges. Original magnification ×140.

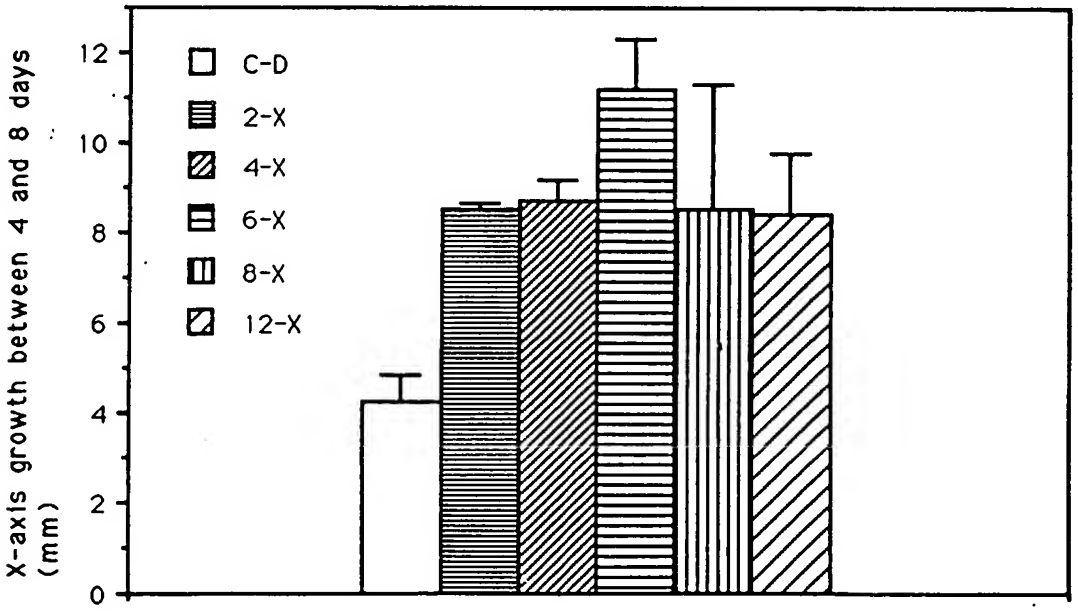

Fig. 8. Graph of RBM colony *x*-axis growth between days 4 and 8 on the surface microgeometries (2-X = 2 μm) compared with control diameter increase (C-D). Student's *t*-tests indicated that the controls were significantly different from all other surfaces at a statistical level of $p < .001$. The 6 μm colonies were different from the 2-, 4-, and 12-μm colonies at a level of $p < .05$ but were not significantly different from the 8-μm colonies. (Error bars = S.D.)

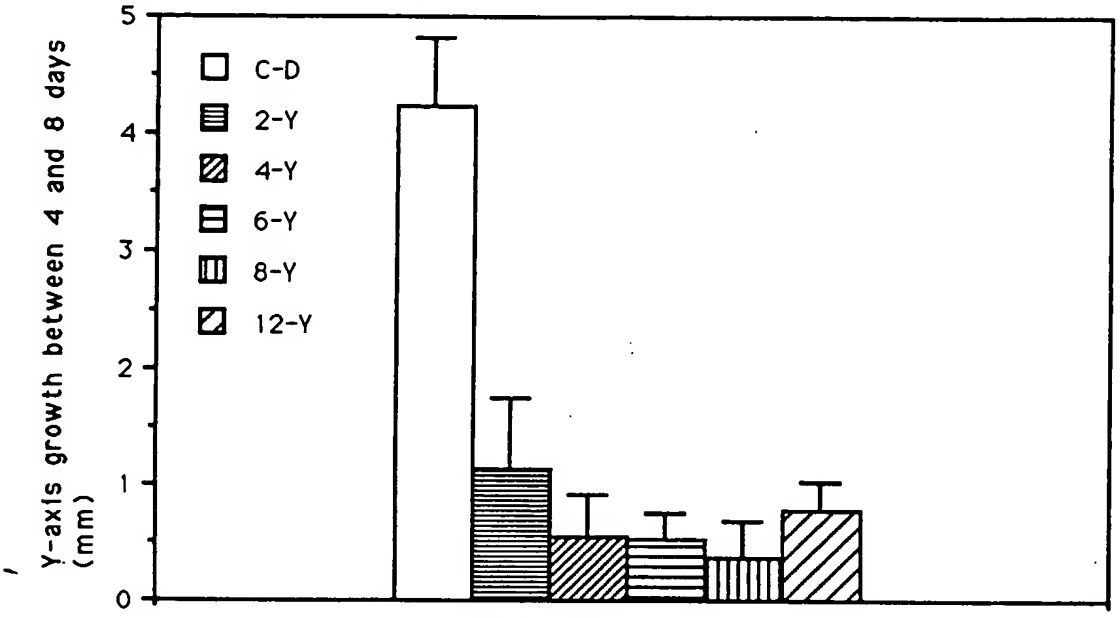

Fig. 9. Graph of RBM colony *y*-axis growth between days 4 and 8 on the surface microgeometries (2-Y = 2 µm) compared with control diameter increase (C-D). Student's *t*-tests indicated that the controls were significantly different from all other surfaces at a statistical level of $p < .001$. The 2-, 4-, 6-, 8-, and 12-µm colonies were not significantly different. (Error bars = S.D.)

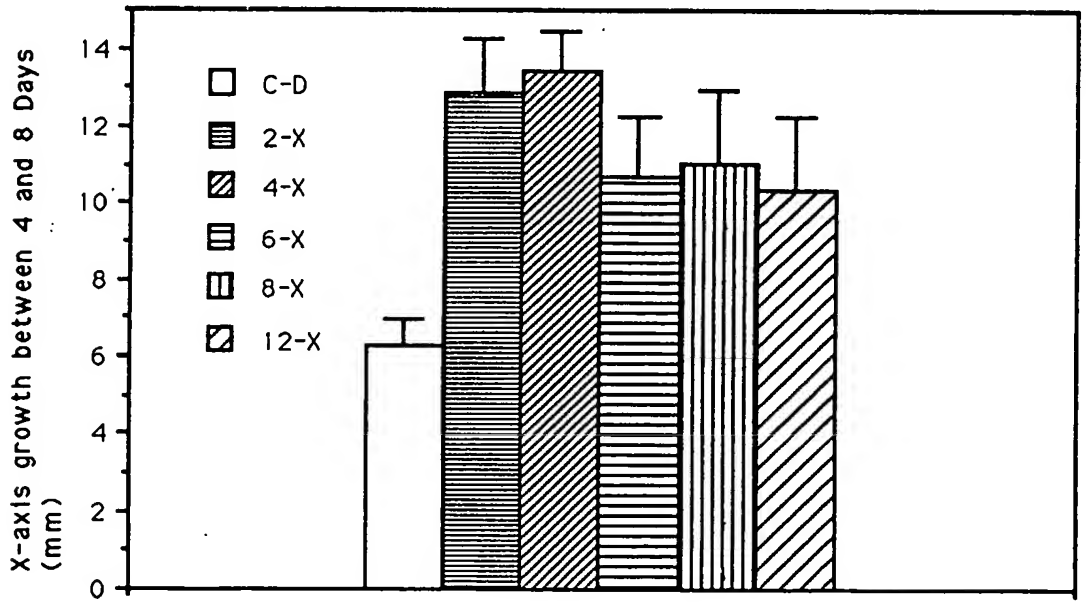

Fig. 10. Graph of RTF colony *x*-axis growth between days 4 and 8 on the surface microgeometries (2-X = 2 µm) compared with control diameter increase (C-D). Student's *t*-tests indicated that the controls were significantly different from all other surfaces at a statistical level of $p < .001$. The 4-µm colonies were different from the 6-, 8-, and 12-µm colonies at a level of $p < .05$ but were not significantly different from the 2-µm colonies. The 2-µm colonies were not significantly different from the 4-, 6-, 8-, and 12-µm colonies. (Error bars = S.D.)

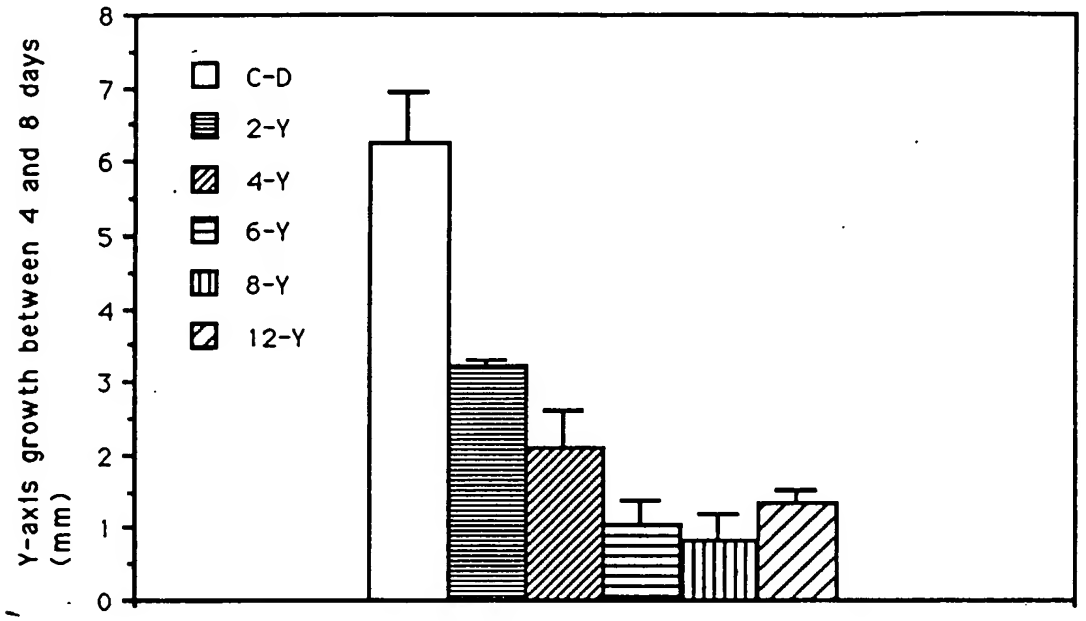

Fig. 11. Graph of RTF colony *y*-axis growth between days 4 and 8 on the surface microgeometries (2-Y = 2 μm) compared with control diameter increase (C-D). Student's *t*-tests indicated that the controls were significantly different from all other surfaces at a statistical level of $p < .001$. The 2-μm colonies were statistically different from the 4-, 6-, 8-, and 12-μm colonies at a level of $p < .01$. The 4-μm colonies were statistically different from the 6-, 8-, and 12-μm colonies at a level of $p < .05$. (Error bars = S.D.)

Fig. 12. Light micrograph of an RBM cell colony on a 2-μm surface after 4 days. The cells have spread extensively, covering several microgrooves each (barely visible at this magnification). While most of the cells are aligned approximately parallel to the surface microgeometry, the orienting influence is not as strong as that observed on the larger microgrooves. Original magnification ×140.

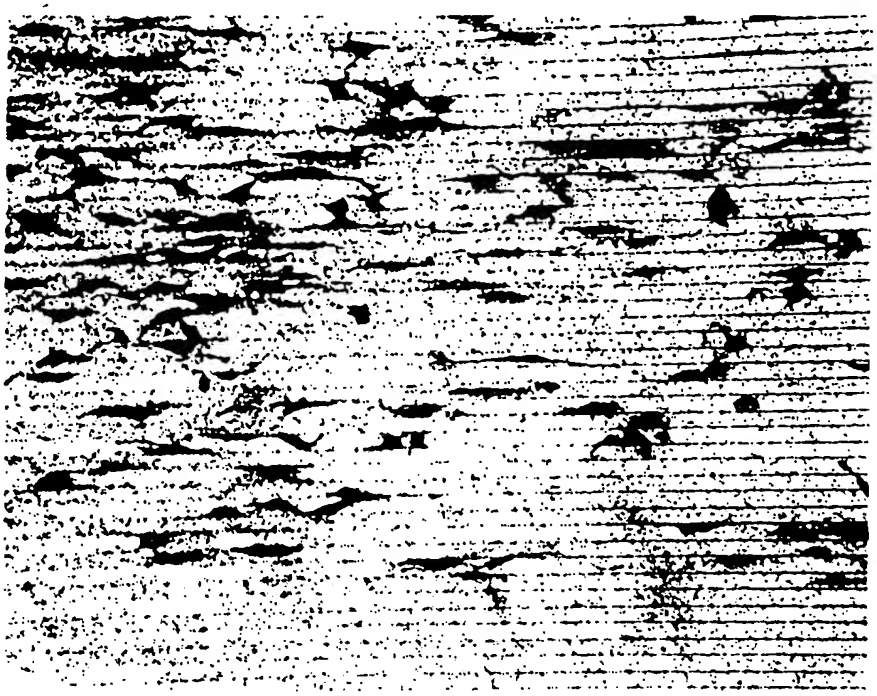

Fig. 13. Light micrograph of an RBM cell colony on a 12-μm surface after 4 days. The cells are spindle-shaped, with some resting within grooves and others on the crests of grooves. Some diagonally oriented cells may be seen on this surface. Original magnification ×140.

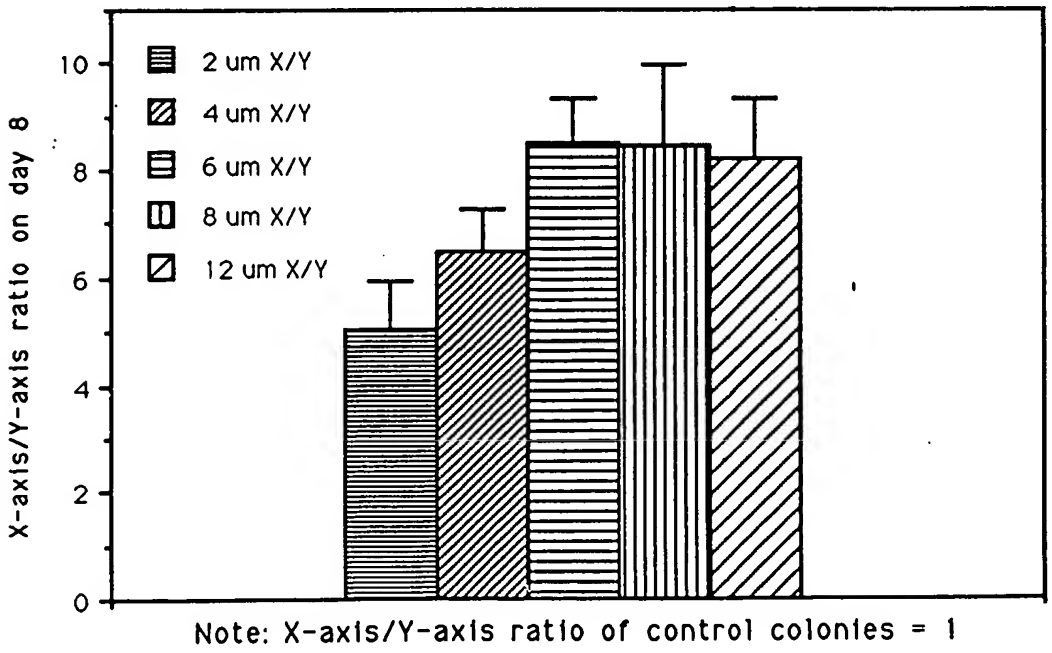

Fig. 14. Graph of RBM cell colony *x*-axis/*y*-axis growth between days 4 and 8 on the surface microgeometries (2-μm *x*/*y* = 2-μm surface). Student's *t*-tests indicated that the 2-μm colonies were significantly different from all other surfaces at a statistical level of $p < .05$. The 4-μm colonies were statistically different from the 6-, 8-, and 12-μm colonies at a level of $p < .05$. (Error bars = S.D.)

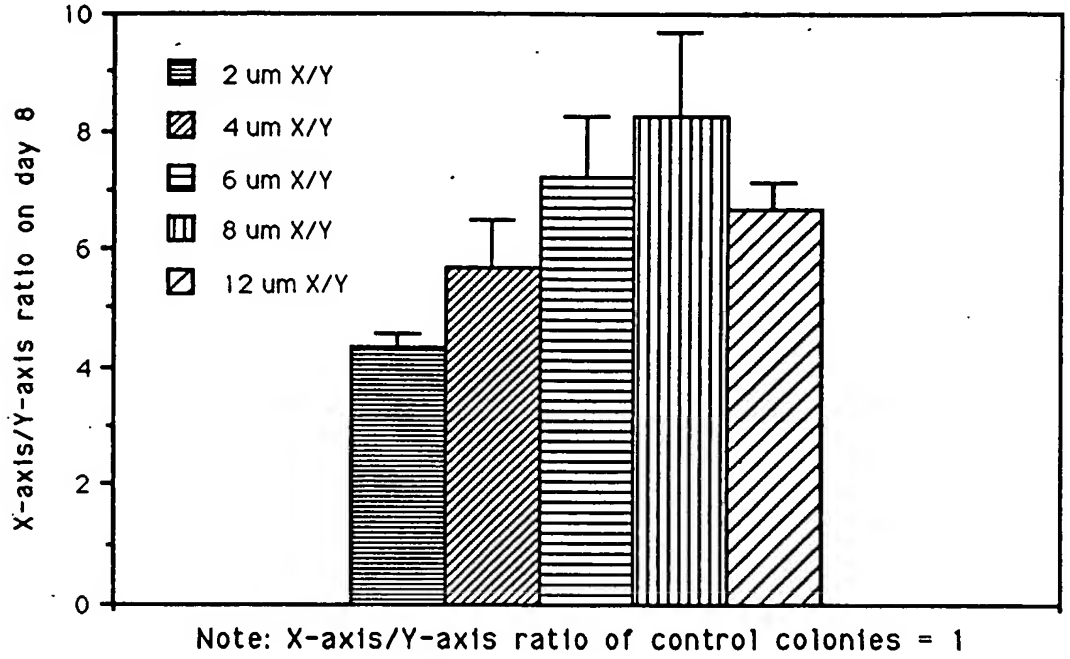

Fig. 15. Graph of RTF cell colony *x*-axis/*y*-axis growth between days 4 and 8 on the surface microgeometries (2-µm *x*/*y* = 2-µm surface). Student's *t*-tests indicated that the 2-µm colonies were significantly different from all other surfaces at a statistical level of $p < .05$. The 4-µm colonies were statistically different from the 8-µm colonies at a level of $p < .01$, but were not significantly different from the 6- and 12-µm colonies. (Error bars = S.D.)

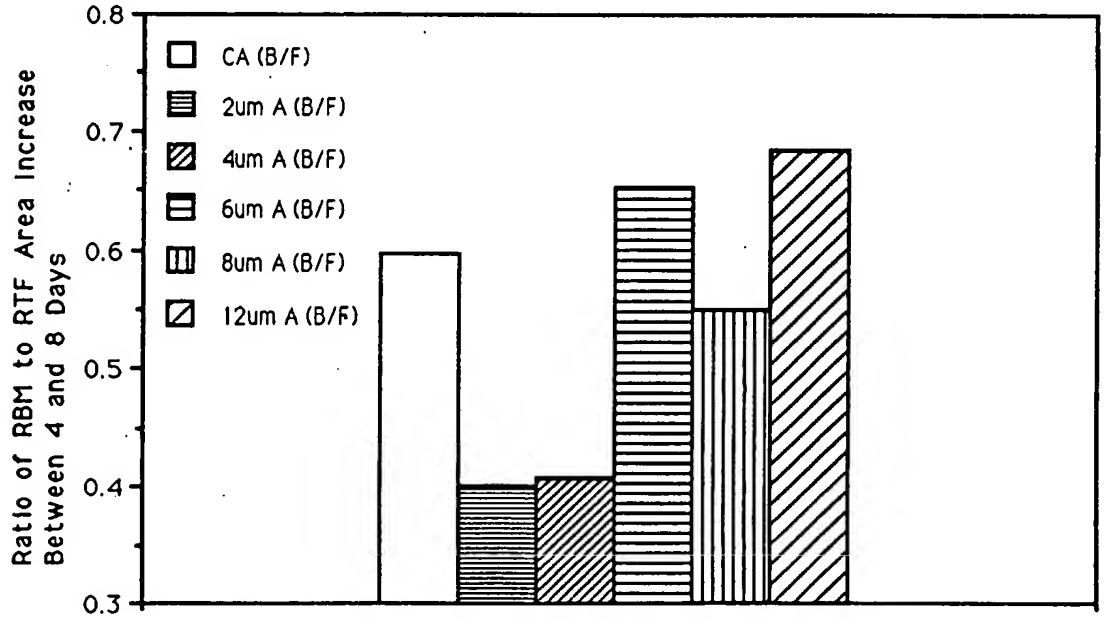

Fig. 16. Graph of the ratio of RBM to RTF cell colony area increase between 4 and 8 days. The lowest ratio is observed on the 2-µm surface, while the highest ratio is observed on the 12-µm surface.

[PROPRIETARY]

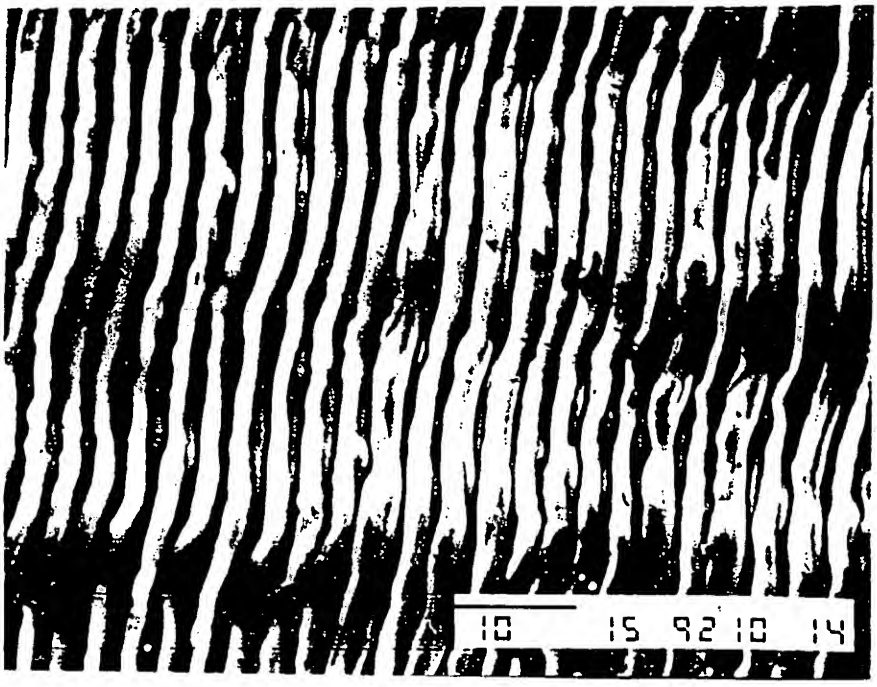

Fig. 17. Scanning electron micrograph of a laser-micromachined surface with small (3-μm) ridges. Bar = 10 μm.

[PROPRIETARY]

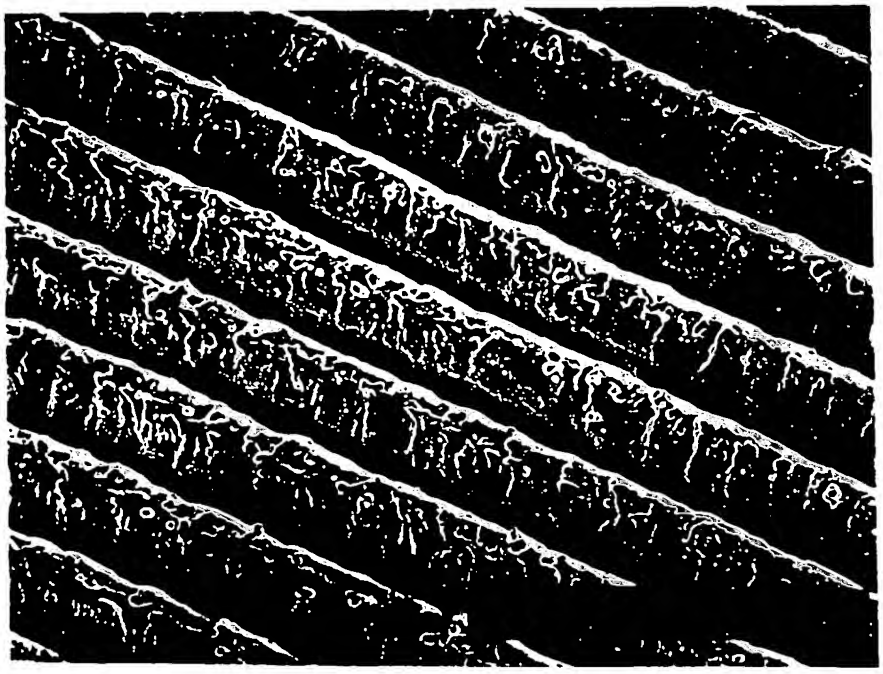

Fig. 18. Scanning electron micrograph of a laser-micromachined surface with large (25-μm) ridges. Bar = 100 μm.